

Spectrum and Dynamics of Optical Frequency Combs Generated with Monolithic Whispering Gallery Mode Resonators

Yanne K. Chembo,* Dmitry V. Strekalov, and Nan Yu

Jet Propulsion Laboratory, California Institute of Technology, 4800 Oak Grove Drive, Pasadena, California 91109, USA

(Received 4 January 2010; published 11 March 2010)

Optical frequency comb generation in whispering gallery mode resonators has been demonstrated in several experiments. The spectra of the combs exhibit a wide variety of complex profiles that are not fully understood. We report a detailed study on frequency comb generation in whispering gallery mode resonators including a complete stability analysis and numerical simulations. We show that the interaction of dispersion and nonlinearity is the key in determining the stability of the comb, the complex characteristics of its spectral profile, and its frequency span. The results will be important for understanding the essential physical processes leading to efficient comb generation.

DOI: 10.1103/PhysRevLett.104.103902

PACS numbers: 42.62.Eh, 42.65.Hw, 42.65.Ky, 42.65.Sf

Spectrally coherent optical frequency combs find ever increasing applications in time-frequency metrology, spectroscopy, sensing, and ultrastable microwave and terahertz generation [1–3]. These combs have been successfully generated with ultrafast mode-locked lasers in the past. However, it has recently been shown that they can also be generated using the whispering gallery modes (WGMs) of a nonlinear monolithic resonator pumped with continuous-wave laser light [4–6]. The strong confinement and high optical quality factor, respectively, lead to high photon density and long photon storage time. Four-wave mixing (FWM) interactions are thereby efficiently enhanced, and lead to comb generation.

The WGM frequency combs show rich spectral characters. In particular, they display certain structure profiles that are not totally intuitive and well understood. The nonlinear interactions inside these resonators are indeed very complex, and have been subject of some extensive studies [7]. Comb generation in WGM resonators has also been discussed and analyzed earlier in the literature. For example, Ref. [8] discussed the threshold behavior in parametric sideband generation. A numerical approach was proposed in Ref. [9], where the light beam in the resonator was analyzed as if propagating along an unfolded periodic trajectory.

These previous studies provided some initial understanding of the comb generation process. However, the spectral profiles and the limited number of generated comb lines remain unclear. In order to provide insight into these critical aspects, we report in this letter a study of the spectrum and dynamics of the comb generation process using a nonlinear dynamics approach. We provide for the first time a complete stability analysis illustrating exactly how the energy from the pump sequentially cascades in the resonator, and excites as much as several hundreds of WGMs. We show that the interaction of the resonator dispersion and nonlinear phase modulation is the key in determining the stability of the comb generation, its

spectral profile, and its frequency span. The results are important for understanding the underlying physical processes and limiting factors that are key for wider spectral span and better stability.

The experimental setup under study is shown in Fig. 1. A millimeter-size calcium fluoride resonator is pumped near 1560 nm by a narrow linewidth (<5 kHz) cw laser. After polarization control, the laser light is coupled into the resonator using an angle-polished optical fiber. The reflected beam at the rim of the resonator is collected by a photodiode to monitor experimentally its Q factor through a ramp modulation of the laser wavelength. Another angle-polished fiber is used to extract the optical frequency comb from the cavity, whose free-spectral range (FSR) is 14.5 GHz. To study the system described above, we will first build a set of coupled rate equations using the slowly-varying amplitude approximation. Then, stability diagrams will be established and numerical simulations performed in order to provide better insight into the comb generation phenomenon.

The nonlinear model.—The orthonormal eigenmodes of a spherical resonator of radius a depend exclusively on the degenerated angular eigennumber ℓ , and on the polarization p (TE or TM). Hence, the eigenmodes $\mathbf{Y}_{\ell p}(\mathbf{r})$ can be

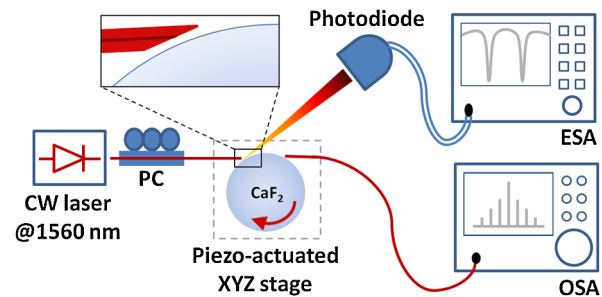


FIG. 1 (color online). Experimental setup. cw: continuous wave; ESA, OSA: electrical, optical spectrum analyzer; PC: polarization controller. The OSA displays the output comb.

explicitly written as $\mathbf{Y}_{\ell, \text{TE}}(\mathbf{r}) \simeq iY_{\ell, \text{TE}}(r, \theta, \phi)\mathbf{e}_\theta$ and $\mathbf{Y}_{\ell, \text{TM}}(\mathbf{r}) \simeq Y_{\ell, \text{TM}}(r, \theta, \phi)\mathbf{e}_r$ with

$$Y_{\ell p}(r, \theta, \phi) = \frac{(-1)^\ell \ell^{1/4} S_{\ell p}(r) e^{-(1/2)\ell[\theta - (\pi/2)]^2} e^{i\ell\phi}}{2^{1/2} \pi^{3/4} \sqrt{\int_0^{+\infty} S_{\ell p}^2(r) r^2 dr}}, \quad (1)$$

where $S_{\ell p}$ is the Debye potential [10]. We expand the electric field as $\mathbf{E}(\mathbf{r}, t) = \sum_\mu \frac{1}{2} \mathcal{E}_\mu(t) e^{i\omega_\mu t} \mathbf{Y}_\mu(\mathbf{r}) + \text{c.c.}$, where $\mu \equiv \{\ell, p\}$ labels the modes of slowly-varying amplitude $\mathcal{E}_\mu(t)$ and frequency ω_μ , while ‘‘c.c.’’ stands for the complex conjugate. We normalize the electric field as $\mathcal{A}_\mu = \sqrt{\epsilon_0 n_0^2 / 2\hbar\omega_\mu} \mathcal{E}_\mu$ where $|\mathcal{A}_\mu|^2$ is the instantaneous number of photons in the mode μ , and n_0 is the real part of the refractive index at the laser frequency Ω_0 . For convenience, we introduce the shifted eigennumber $l = \ell - \ell_0$, where ℓ_0 is the angular number of the central (or pumping) mode. The eigenfrequencies therefore read $\omega_l \simeq \omega_0 + [c/n_0 a]l$.

To obtain the modal equations, we introduce the field expansion into a wave equation characterized by a refractive index $n_0(\omega) + \Delta n(\omega, \|\mathbf{E}\|^2)$, where $n_0(\omega)$ contains chromatic dispersion, while the excess index $\Delta n = -in_Q(\omega) + \frac{1}{2}n_2 n_0 \epsilon_0 c \|\mathbf{E}\|^2$ accounts for the frequency-dependent losses (through n_Q) and for the FWM (through n_2). The spatiotemporal variations of this global equation are projected onto $\mathbf{Y}_\eta^*(\mathbf{r}) e^{-i\omega_\eta t}$ (hermitian inner product), and we finally obtain the following coupled rate equations for the modal field dynamics:

$$\dot{\mathcal{A}}_\eta = -\frac{1}{2} \Delta\omega_\eta \mathcal{A}_\eta + \frac{1}{2} \Delta\omega_\eta \delta_{\eta 0} \mathcal{F}_0 e^{i\sigma t} - ig_0 \sum_{\alpha, \beta, \mu} \Lambda_\eta^{\alpha\beta\mu} \mathcal{A}_\alpha \mathcal{A}_\beta^* \mathcal{A}_\mu e^{i\varpi_{\alpha\beta\mu\eta} t}. \quad (2)$$

In Eq. (2), $\Delta\omega_\eta = 2\Gamma_\eta \omega_\eta n_Q(\omega_\eta) / n_0$ is the modal bandwidth, where $\Gamma_\eta = \int_V \|\mathbf{Y}_\eta\|^2 dV$ is the modal confinement factor. The effective volume of the central mode is $V_0 = [\int_V \|\mathbf{Y}_0\|^4 dV]^{-1}$, and $g_0 = n_2 c \hbar \omega_0^2 / n_0^2 V_0$ is the FWM gain at ω_0 . The intermodal coupling factor

$$\Lambda_\eta^{\alpha\beta\mu} = \frac{\omega_\mu^2}{\omega_0^2} \sqrt{\frac{\omega_\alpha \omega_\beta \omega_\mu}{\omega_\eta^3}} \frac{\int_V [\mathbf{Y}_\eta^* \cdot \mathbf{Y}_\mu][\mathbf{Y}_\beta^* \cdot \mathbf{Y}_\alpha] dV}{\int_V \|\mathbf{Y}_0\|^4 dV} \quad (3)$$

defines the coupling strength between the four interacting modes α, β, μ , and η , and it depends on their power density overlap. As indicated by the Kronecker symbol $\delta_{\eta 0}$, the external field \mathcal{F}_0 is only resonant with the mode $l = 0$, with a detuning $\sigma = \Omega_0 - \omega_0$. The ideal resonance condition occurs when the modal FWM frequency detuning $\varpi_{\alpha\beta\mu\eta} = \omega_\alpha - \omega_\beta + \omega_\mu - \omega_\eta$ vanishes, and it corresponds to the FWM interactions $\hbar\omega_\alpha + \hbar\omega_\mu \rightarrow \hbar\omega_\beta + \hbar\omega_\eta$ for which the energy and the total angular momentum of the interacting photons are conserved ($\ell_\alpha + \ell_\mu = \ell_\beta + \ell_\eta$). This ideal condition is automatically fulfilled

in a dispersionless cavity with perfectly equidistant eigenmodes. However, a detailed calculation shows that in presence of second-order dispersion, the intermodal detuning ‘‘walks-off’’ following $\varpi_{\alpha\beta\mu\eta} = \frac{1}{2} \zeta [l_\alpha^2 - l_\beta^2 + l_\mu^2 - l_\eta^2]$, where

$$\zeta = -\xi_1 \frac{2^{\frac{3}{2}} c}{9 n_0 a} \ell_0^{-5/3} - \frac{2n'_\omega + \omega_0 n''_\omega}{n_0} \left[\frac{c}{n_0 a} \right]^2 \quad (4)$$

is the cavity dispersion parameter, and $\xi_1 = 2.338$ is the first zero of the Airy function. This parameter can be positive or negative (anomalous and normal dispersion, respectively), and it includes both geometrical and material contributions.

Stability analysis.—The first step of our stability analysis is to study the threshold mechanism in comb generation. Below threshold ($\mathcal{A}_l \equiv 0$ for $l \neq 0$), the steady-state optical power $|\mathcal{A}_{0s}|^2$ of the central mode $l = 0$ obeys

$$|\mathcal{F}_0|^2 = \frac{4g_0^2}{\Delta\omega_0^2} |\mathcal{A}_{0s}|^6 + \frac{8g_0\sigma}{\Delta\omega_0^2} |\mathcal{A}_{0s}|^4 + \left[1 + \frac{4\sigma^2}{\Delta\omega_0^2} \right] |\mathcal{A}_{0s}|^2. \quad (5)$$

This equation is bicubic and for a given input $|\mathcal{F}_0|^2$, there may be one, two, or three solutions (hysteresis) for $|\mathcal{A}_{0s}|^2$. In case of hysteresis, only the values of \mathcal{A}_{0s} for which $\mathbf{C} = \partial[|\mathcal{F}_0|^2] / \partial[|\mathcal{A}_{0s}|^2] > 0$ are stable and can be experimentally observed.

On the other hand, a given sidemode pair $\mathcal{A}_{\pm l}$ is excited at threshold through degenerate FWM *via* \mathcal{A}_0 when the perturbations $\delta\mathcal{A}_{\pm l}$ obeying

$$\delta\dot{\mathcal{A}}_{\pm l} = -\frac{1}{2} \Delta\omega_{\pm l} \delta\mathcal{A}_{\pm l} - ig_0 [\Lambda_{\pm l}^{\pm l, 0, 0} + \Lambda_{\pm l}^{0, 0, \pm l}] |\mathcal{A}_0|^2 \delta\mathcal{A}_{\pm l} - ig_0 \Lambda_{\pm l}^{0, \mp l, 0} \mathcal{A}_0^2 \delta\mathcal{A}_{\mp l}^* e^{i\varpi_{\pm l} t} \quad (6)$$

are diverging (positive eigenvalues), with $\varpi_l \equiv \varpi_{0, l, 0, -l}$. We have solved these perturbation equations, and found that for nearly degenerated modal parameters, the sidemode pair $\mathcal{A}_{\pm l}$ is excited when $\mathbf{S}(l) < 0$, with

$$\mathbf{S}(l) = 12[g_0 |\mathcal{A}_{0s}|^2]^2 + 8[2\sigma + \varpi_l][g_0 |\mathcal{A}_{0s}|^2] + [2\sigma + \varpi_l]^2 + \Delta\omega_0^2. \quad (7)$$

Hence, stable optical sidemode pairs are generated when the conditions $\mathbf{C} > 0$ for the central mode and $\mathbf{S}(l) < 0$ for at least one sidemode pair are fulfilled simultaneously. This double condition can be explicitly translated as

$$\text{Stability for } l = 0: |\mathcal{A}_{0s}|^2 \notin [\mathbf{B}_-(0), \mathbf{B}_+(0)],$$

$$\text{Stability for } l \neq 0: |\mathcal{A}_{0s}|^2 \in [\mathbf{B}_-(l), \mathbf{B}_+(l)], \quad (8)$$

where the stability boundaries are explicitly defined by

$$\mathbf{B}_\pm(l) = \frac{1}{3g_0} \left[-2\sigma_l \pm \sqrt{\sigma_l^2 - \frac{3}{4} \Delta\omega_0^2} \right] \quad (9)$$

with $\sigma_l = \sigma - \frac{1}{2}\zeta l^2$. We can also determine the threshold power for comb generation as the minimum of the lower boundary following $\partial \mathbf{B}_- / \partial \sigma_l = 0$, which yields

$$|\mathcal{A}_{0l}|_{\text{th}}^2 = \frac{1}{2} \frac{\Delta \omega_0}{g_0} = \frac{1}{2\hbar\omega_0} \frac{n_0^2}{n_2 c} \frac{V_0}{Q_0}, \quad (10)$$

where Q_0 is the optical quality factor of the central mode. This expression for the threshold is different from that in Ref. [8], because our model considers the more general case where any sidemode pair can be excited at threshold (and not only the modes adjacent to the pump). This first sidemode pair $\pm l$ oscillating at threshold is solution of $\partial \mathbf{B}_- / \partial l = 0$, yielding $|l| = l_{\text{th}}(\sigma) = \{(2/\zeta) \times [\sigma + \Delta \omega_0]\}^{1/2}$, to be rounded to the nearest integer. This threshold oscillating sidemode pair can therefore be selected by tuning the laser offset σ , or by tuning $\Delta \omega_0$ through coupling.

Results and discussion.—The above stability analysis shows that when there is no cavity dispersion [$\zeta = 0$], we have $\mathbf{B}_{\pm}(l) \equiv \mathbf{B}_{\pm}(0)$. Hence, for all l , the conditions of Eq. (8) cannot be fulfilled because the instability area for the central mode exactly overlaps the stability zone for the sidemodes. A nonzero dispersion is therefore *necessary* for comb generation [9]. This is similar to supercontinuum generation in nonlinear fibers [11]. Naturally, a too large dispersion ζ would lead to essentially unequidistant modes, incompatible with comb generation. An example of stability diagram corresponding to the conditions of Eq. (8) is illustrated in Fig. 2. It appears that only a pair of symmetrical bands of modes can be *directly* excited by the pump through *degenerate* FWM interactions of the kind $\hbar\omega_0 + \hbar\omega_0 \rightarrow \hbar\omega_l + \hbar\omega_{-l}$. They are unexpectedly not always adjacent to the central mode. For example, if the central mode is pumped twice above threshold, then only the modes such that $52 < |l| < 83$ can be excited by the pump (dark shaded bands in Fig. 2). We refer to these modes as the *primary comb*. Because of this bandlike structure, degenerate FWM cannot efficiently excite a

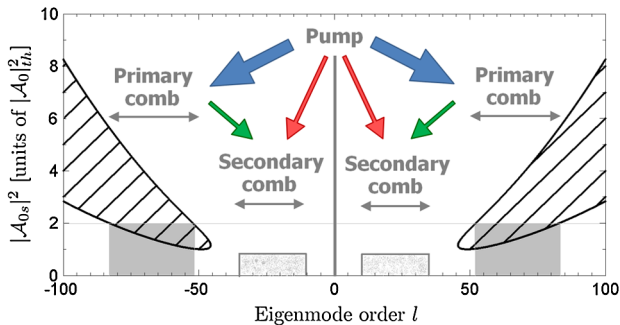


FIG. 2 (color online). Stability diagram as a function of eigenmode order l and power $|\mathcal{A}_{0s}|^2$ in the central mode. The hatched area corresponds to stable primary comb generation. The parameters are $a = 2.3$ mm, $n_2 = 3.2 \times 10^{-20}$ m² W⁻¹, $n_0 = 1.43$, $Q_0 = 8 \times 10^8$, $V_0 = 7 \times 10^{-12}$ m³, $\lambda_0 = 1560.3$ nm, with $\sigma = 0$ and $\zeta/2\pi = 200$ Hz (anomalous dispersion).

wide comb of adjacent WGMs. On the other hand, *non-degenerate* FWM interactions, i.e., bichromatic comb generation [12] is very efficient and does not have a threshold condition. The cascaded interactions between the pump, the primary and the subsequent higher order combs can efficiently generate the full comb, as indicated by the arrows in Fig. 2.

To further illustrate this physical process, we carried out some extensive numerical simulations of the comb generation. We used the experimental parameters in Eq. (2), and we have generated a time sequence of snapshots of the comb generation process as shown in Fig. 3. This spectrotemporal representation shows that at $8 \mu\text{s}$, only the primary comb lines are generated. After $35 \mu\text{s}$, however, the comb lines start to fill the entire spectral region, resulting from nondegenerate FWM. High efficiency of nondegenerate FWM is here necessary because the generation of a large set of coherent and equidistant comb lines is not possible through degenerate FWM. Our simulation also suggests that a wide-span coherent comb may not necessarily have all the resonator modes filled in between. A sparse but wide comb is advantageous from the perspective of the total pump power required for generating a wide comb.

To validate our model, we compare the simulated spectra with those obtained experimentally with the set-up of Fig. 1. The adjustable parameters of the model were the resonator dispersion and pump light intensity. Figure 4(a) shows an example of the experimentally observed comb profile displaying a distinctive spectral signature. It is successfully reproduced in the numerical simulation as it can be seen in Fig. 4(b), and this agreement confirms the analytical stability study. The most strongly excited modes are within the primary comb stability band, while a *sub-harmonic* secondary comb is created at mid-distance from the pump. It should be emphasized that all spectral features

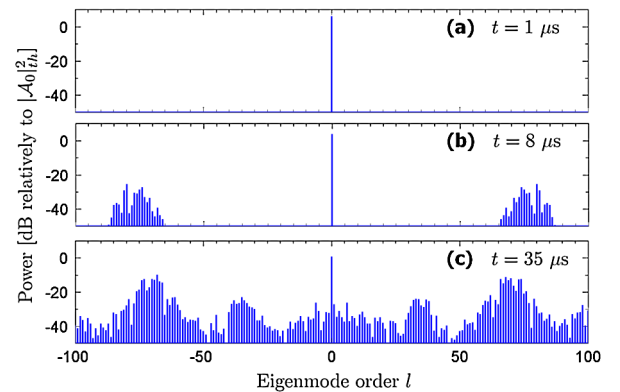


FIG. 3 (color online). Evidence of the sequentially cascading comb excitation for $|\mathcal{A}_{0s}|^2 = 2.5|\mathcal{A}_{0l}|_{\text{th}}^2$. (a) First, the central mode is excited above threshold by the photons from the external pump; (b) Then, the central mode excites the primary comb through degenerate FWM; (c) Finally, the pump uses the primary comb as a relay to excite the secondary and higher order combs through nondegenerate FWM, thereby filling the gaps.

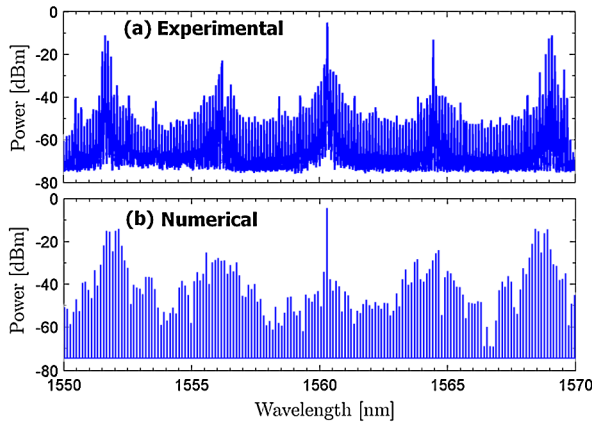


FIG. 4 (color online). (a) Experimental spectrum; (b) snapshot of the simulated spectrum at $t = 1$ ms, with $|\mathcal{A}_{0s}|^2 = 2.5|\mathcal{A}_{0th}|^2$.

(modulation depths, position of extrema, etc.) are quite accurately recovered with the model, despite the extremely large amplitude window (80 dB), wide wavelength span (20 nm), and huge number of modes (~ 200). This analysis also explains the multiple FSR spacing and periodic spectral modulation previously observed in WGM combs [5,6]. It is also noteworthy that the numerical simulations in Ref. [9] using a discrete iterative map model do also yield comb spectra with the modulated structure of Fig. 4.

With the time-dependent simulation capability, it is also possible to investigate the spectro-temporal dynamics of the comb, as shown in Fig. 5. At $t = 0$, the system starts from the vacuum ground state with $\langle |\mathcal{A}_l(0)|^2 \rangle = \frac{1}{2}$, where the brackets stand for ensemble average over l . The comb displays a chaotic dynamics, with a maximal Lyapunov exponent $\tilde{\lambda} \approx 8.4 \times 10^4 \text{ s}^{-1}$ (i.e., the temporal dynamics of the comb cannot be predicted beyond $\tilde{\lambda}^{-1} \approx 12 \mu\text{s}$). This chaotic amplitude dynamics induces parasitic modulation sidebands that may be detrimental for phase coherence. However, lower pump values (typically below twice the threshold) lead to stationary states with constant amplitudes, or to *harmonic* secondary combs with multiple FSR spacing. One of the challenges in WGM comb generators is to expand the spectral span to one octave. A large FSR (>1 THz) makes it easier to achieve a wider comb span because of a reduced number of modes. However, for most applications, FSRs smaller than 10 GHz are desirable, and they would correspond to combs with roughly 10000 modes. Our model suggests that widening the span of the comb can be achieved by optimizing the position of the primary comb relatively to the dispersion curve, which is known to vary nonmonotonously with wavelength in most media. This optimization can be done in the general case through Eq. (6). The approach thereby provides a useful tool for the generation of a wider comb span. In particular, it enables the determination of a

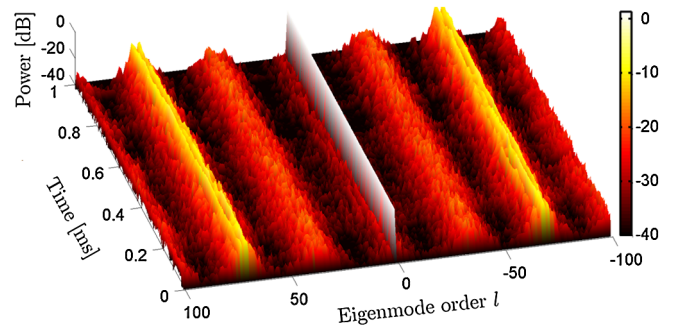


FIG. 5 (color online). Spectrotemporal representation of the comb dynamics. Note that Fig. 4(b) is the snapshot at $t = 1$ ms.

suitable dispersion compensation scheme or an optimal geometry leading to the widest combs possible.

In conclusion, we have presented a joint theoretical and experimental study on optical frequency comb generation with monolithic WGM resonators. We have shown that the interaction between dispersion and Kerr nonlinearity affects the spectrum of the generated comb. In particular, we have shown that the pump first excites a primary comb through degenerate FWM, and then cascades out secondary combs through nondegenerate FWM. The results are in excellent agreement with experimentally observed spectral profiles. The theoretical analysis and numerical simulation helped to understand the sequence of the cascading process leading to the excitation of huge numbers of modes in WGM resonators. They indicated that the comb can lose its spectral stability and become chaotic for strong pumping. These analyses will be helpful for engineering the comb spectra, and for further investigations on the effects of stochastic noise.

This work was performed at the Jet Propulsion Laboratory, California Institute of Technology, under a contract with NASA. Part of this research was funded by the NASA Postdoctoral Program, administered by Oak Ridge Associated Universities (ORAU).

*yanne.chembo@jpl.nasa.gov

- [1] S. T. Cundiff and J. Ye, *Rev. Mod. Phys.* **75**, 325 (2003).
- [2] J. L. Hall, *Rev. Mod. Phys.* **78**, 1279 (2006).
- [3] T. W. Hänsch, *Rev. Mod. Phys.* **78**, 1297 (2006).
- [4] P. Del'Haye *et al.*, *Nature (London)* **450**, 1214 (2007).
- [5] A. Savchenkov *et al.*, *Phys. Rev. Lett.* **101**, 093902 (2008).
- [6] I. S. Grudin *et al.*, *Opt. Lett.* **34**, 878 (2009).
- [7] K. Vahala, *Nature (London)* **424**, 839 (2003), and refs. therein.
- [8] A. Savchenkov *et al.*, *Phys. Rev. Lett.* **93**, 243905 (2004).
- [9] I. H. Agha *et al.*, *Opt. Express* **17**, 16209 (2009).
- [10] B. R. Johnson, *J. Opt. Soc. Am. A* **10**, 343 (1993).
- [11] J. M. Dudley *et al.*, *Rev. Mod. Phys.* **78**, 1135 (2006).
- [12] D. Strekalov and N. Yu, *Phys. Rev. A* **79**, 041805(R) (2009).